PACS:61.43.Gt; 68.03.–g; 68.43.–h; 81.40.Ef doi: 10.15407/Surface.2022.14.159

HYBRID COMPOSITES PREPARED BY CARBONIZATION OF ACETYLACETONE AND METAL ACETYLACETONATES ON A SURFACE OF SILICA GEL

V.M. Gun'ko,[1]J.Skubiszewska-Zięba,[2]B. Charmas[2]

[1]Chuiko Institute of Surface Chemistry, 17 General Naumov Street, 03164 Kyiv, Ukraine
e–mail: vlad_gunko@ukr.net
[2]Faculty of Chemistry, Maria Curie-Skłodowska University, 3 Maria Curie-Skłodowska Sq., 20-031 Lublin, Poland

Hybrid adsorbents with carbon/silica, carbon/metal oxide/silica, and carbon/metal/silica could be of interest from a practical point of view since they can effectively adsorb both polar and nonpolar compounds. Therefore, mesoporous silica gel Si–60 modified by carbonization acetylacetone or Ti, Zn, Ni, Co, Cr, Zr acetylacetonates has been studied using nitrogen and water adsorption–desorption, thermogravimetry, transmission electron microscopy, X–ray diffraction, and X–ray fluorescence methods. Grafted C/X phases consist of metal compounds (X denotes metal oxide or silicate or/and metal) and char, whose characteristics can be varied changing metal in the precursors and their amounts. The morphological, structural, and textural characteristics of C/X/SiO₂, such as composition and particle size distributions of deposits, a number and kind of polar and non polar surface sites, specific surface area, pore volume, and pore size distributions depend on the type, content, and distribution of the C/X deposits. The changes in the grafted matters occur with increasing precursor and C/X concentrations and a possible catalytic effect of the X phases on the carbonization reactions. Appropriate selection of precursor structure and amounts allows one to vary and control the characteristics of whole hybrid adsorbents that is of importance from a practical point of view.

Keywords**:** *mesoporous silica gel, metal acetylacetonate carbonization, carbon deposits, carbon/metal compound deposits, deposit morphology, textural characteristics, water desorption*

Introduction

The adsorption characteristics of various hybrid adsorbents composed of polar and nonpolar, hydrophilic and hydrophobic phases or surface patches at substrates could be more appropriate for certain practical applications in comparison to simple adsorbents such as silicas [1–12]. To prepare different hybrid adsorbents and to change their morphological, structural, textural, and adsorption characteristics, various modification techniques can be applied to different substrates such as silicas, porous (silica gels, precipitated silicas) or highly disperse (fumed or fuse silicas), etc.[13–57]. One of these techniques is the carbonization of organics or more complex precursors on the substrates that results in the formation of carbon or more complex deposits with well controlled characteristics[4,14,36–57]. Typically, pure pyrocarbons (chars) in hybrid adsorbents possess a relatively small number of active sites (e.g., oxidized functionalities), which could play an important role in bonding of polar molecules in different media. This is caused by the morphology of the carbon layers mainly of nonpolar pregraphite, turbostratic structures with amorphized small basal planes of sizes from one to several nanometers similar to those in individual carbon blacks, chars, and activated carbons [1–14]. To increase the amounts of active sites on hybrid adsorbent surfaces, additional oxidizing of chars with formation of COH, C=O, COOH and other functionalities, mixed X/SiO_2 as substrates (possessing a larger number of active sites than parent silica has [4,14]), or organometallics as C/X precursors [38,46] can be utilized. The deposit

structures generated upon the carbonization of organometallics could be more complex than that of chars formed upon the carbonization of pure organics due to the formation of additional X phases with metal oxide, silicate, or/and metal [38]. It is known that the carbonization of organometallics on various substrates results in the formation of C/X of different structures affected not only by the specific surface area and porosity but also by surface chemistry of the substrates[38,46]. Clearly, the presence of carbon/metal compounds can change not only the topology and morphology but also other characteristics of $C/X/SiO_2$ adsorbents, such as surface site distribution, catalytic and adsorption abilities, pore size distribution, porosity, etc. It should be noted that $C/X/SiO_2$ adsorbents prepared using pyrolysis of organometallic precursors have not been adequately explored in comparison to C/SiO_2 materials synthesized utilizing pure organics as char precursors [1–57]. Therefore, the aim of this work was to synthesize $C/X/SiO_2$ materials utilizing silica gel as a substrate modified upon the carbonization of various organometallics and to investigate the whole adsorbents using adsorption–desorption of nitrogen and water, thermogravimetry, spectroscopic and microscopic methods to elucidate the impact of the nature of metals in $M(AcAc)_n$ on the morphological, structural, textural, and adsorption characteristics of whole $C/X/SiO_2$ adsorbents.

Experimental

Materials

Mesoporous silica gel Si–60 (Merck) was used as a substrate to prepare carbon/X/silica materials (carbosils, CS_X, where X denotes a metal in the phases formed during pyrolysis of the precursors). Silica gel Si–60 (SG) was washed away from surface mineral impurities with 18% HCl solution in a Soxhlet apparatus and then with distilled water. Then silica gel was dried at 200 °C for 24 h and cooled in a dessicator before pyrolysis of acetylacetonates (AcAc) of zirconium [$Zr(AcAc)_4$], titanium [titanyl $TiO(AcAc)_2$], nickel [$Ni(AcAc)_2$], zinc [$Zn(AcAc)_2$], chromium [$Cr(AcAc)_3$], and cobalt [$Co(AcAc)_2$] (Aldrich) immobilized on silica gel using the impregnation method. A given acetylacetonate (0.01 M) was deposited on 5 g of the silica gel from methanol (250 mL) sonicated for uniform distribution of organometallics; and then methanol was removed on degassing in vacuum.

Pyrolysis of acetylacetonates deposited on silica gel was carried out in an autoclave (0.3 dm^3) with stainless steel at 500 °C for 6 h. After the carbonization, samples were washed in the Soxhlet apparatus with N,N–dimethylformamide and acetone to remove uncarbonized compounds, and then dried at 200 °C in the deoxygenated nitrogen flow. The hybrid adsorbents were labeled as CS_{Ti}, CS_{Cr1}, CS_{Co}, CS_{Ni}, CS_{Zn}, and CS_{Zr1} (Table 1).

Table 1. Concentrations of grafted metal compounds and char

Sample	Metal compounds	Content of metal compounds, wt.%	Structure (crystallite size)	Carbon content, wt.%	$C_\Sigma = C_C + C_X$, wt.%
CS_{Ti}	TiO_2	11.37	Anatase (~11 nm)	9.2	20.57
CS_{Cr1}	Cr_2O_3 ()	11.26	Amorphous	12.0	23.26
CS_{Cr2}	Cr_2O_3 (amorph.)	8.28	Amorphous	4.8	13.08
CS_{Co}	Co	8.42	Metallic Co (20–25 nm)	6.1	14.52
CS_{Ni}	Ni, NiO	9.42	Ni (25 nm), NiO (~13 nm)	5.9	15.32
CS_{Zn}	Zn_2SiO_4	10.98	Zn silicate	6.5	16.48
CS_{Zr1}	ZrO_2	17.14	XRD amorphous	13.8	30.94
CS_{Zr2}	ZrO_2	10.19	Partially crystalline (~4 nm)	7.4	17.59
CS1	–	–	–	4.0	4.0
CS2	–	–	–	9.1	9.1
CS3	–	–	–	14.5	14.5

The utilization of the same amounts (0.01 M) of metal acetylacetonates results in deposition of equal amounts of metal moles but different amounts of moles of acetylacetonate groups, since the n values in $M(AcAc)_n$ compounds are different (n = 2–4). Therefore, the metal valence in

M(AcAc)$_n$ was taken into consideration and 2/3×0.01 M of chromium acetylacetonate (CS_{Cr2}) and 2/4×0.01 M of zirconium acetylacetonate (CS_{Zr2}) were additionally utilized. Three C/silica samples labeled as CS1, CS2, and CS3 were prepared using acetylacetone (L. Light Co.) as a precursor in the amounts of 0.02, 0.03, and 0.04 M, respectively, per 5 g of pristine silica gel (Table 1).

Nitrogen adsorption–desorption isotherms and textural characteristics

Low–temperature (77.35 K) nitrogen adsorption–desorption isotherms were recorded using a Sorptomat 1900 (Carlo–Erba, Milan) adsorption analyzer. The specific surface area (S_{BET}) was calculated using the standard BET equation [58] at p/p_0 between 0.06 and 0.2 (where p and p_0 denote the equilibrium and saturation pressures of nitrogen, respectively). The pore volume (V_p) was estimated under the relative pressure $p/p_0 \approx 0.98$ [59].

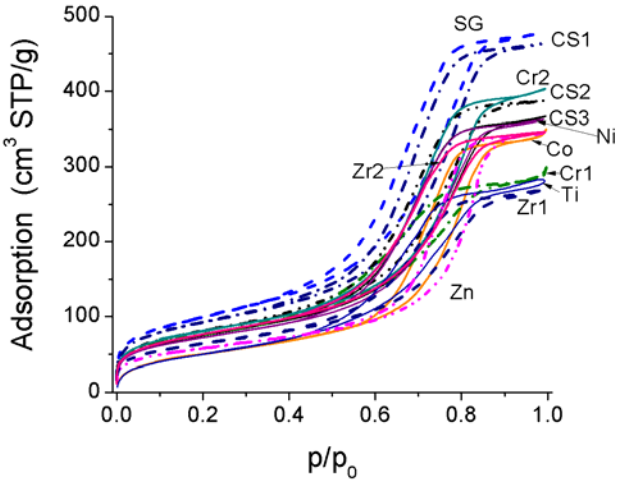

Fig. 1. Nitrogen adsorption-desorption isotherms for Si-60 and composites

The nitrogen desorption data were used to compute the pore size distributions (PSD, differential $f_V(R) \sim dV_p/dR$ and $f_S(R) \sim dS/dR$) using a self–consistent regularization (SCR) procedure under non–negativity condition ($f_V(R) \geq 0$ at any pore radius R) at a fixed regularization parameter $\alpha = 0.01$. A complex pore model was applied with slit–shaped (S) pores in carbon and cylindrical (C) pores in silica and voids (V) between spherical carbon or metallic nanoparticles packed in random aggregates (pore models used SCV, VCV, or CV with SCR method) with the density functional theory (DFT) method [60–62]. The differential PSD with respect to the pore volume $f_V(R) \sim dV/dR$, $\int f_V(R)dR \sim V_p$ were recalculated to incremental PSD (IPSD) at $\Phi_V(R_i) = (f_V(R_{i+1}) + f_V(R_i))(R_{i+1} - R_i)/2$ at $\sum \Phi_V(R_i) = V_p$. The $f_V(R)$ and $f_S(R)$ functions were also used to calculate contributions of nanopores (V_{nano} and S_{nano} at radius in the range of 0.35 nm $< R \leq$ 1 nm), mesopores (V_{meso} and S_{meso} at 1 nm $< R \leq$ 25 nm), and macropores (V_{macro} and S_{macro} at 25 nm $< R \leq$ 100 nm) [60]. Additionally, non–local DFT method (NLDFT, Quantachrome software, with a model of cylindrical pores in silica or slit/cylindrical pores in carbon) [63] was used to calculate the differential PSD with respect to the pore volume and specific surface area. The average values of the pore radii $\langle R_x \rangle$ were determined with respect to the pore volume (x = V) and specific surface area (x = S), respectively, as the ratio of the first and zero moments of the related distribution functions

$$\langle R_x \rangle = \int_{R_{min}}^{R_{max}} R f_x(R) dR \Big/ \int_{R_{min}}^{R_{max}} f_x(R) dR . \qquad (1)$$

XRD and XRF

XRD measurements were performed using a Siemens D 5000 powder diffractometer with Cu K_α radiation in step scan mode (2θstep size of 0.04°, counting time of 2 s per step, 2θ range of 2 – 80°). To identify the structure of synthesized deposits, the XRD patterns were compared to those of known compounds from the JPCDS–ISDD files. Additionally, metal concentration in X phase of C/X/SiO_2 was determined using a XRF (Canberra) spectrometer with the radioactive sources of Fe^{55} and Cd^{109}. Obtained results are summarized in Table 1.

Thermogravimetric measurements

Thermal decomposition of carbon/mineral adsorbents was investigated over the 293–1273 K range by means of thermogravimetry (TG) with differential thermal analysis (DTA) in air to determine the carbon concentration in the composites using a Derivatograph C (Paulik, Paulik&Erdey, MOM, Budapest) at a heating rate of 10 K/min. Thermodesorption of water was studied under quasi–isothermal conditions. Water vapor was adsorbed on carbosils (≈1 g) in a dessicator containing liquid bidistilled water at room temperature for 72 h. Wetted samples were heated to 573 K using the TG method.

Transmission Electron Microscopy

TEM images of the samples were recorded using a BS 540 (Tesla) apparatus (accelerating voltage 80 kV, resolution 0.8 nm, magnification ×12000 or ×20000). Microscope samples of C/X were prepared using the platinum–carbon replication method with evaporation of carbon and platinum onto the adsorbent surface then treated in hydrofluoric acid to dissolve oxides.

Results and discussion

According to XRD data (Table 1, XRD patterns are not shown here), cobalt in CS_{Co}represents a metallic phase (crystallite size of 20–25 nm) due to its reduction during carbonization of $Co(AcAc)_2$. Nickel in CS_{Ni} is in both metallic (crystallite size ~25 nm) and oxide (~13 nm) phases. CS_{Cr} contains amorphous chromium oxide. During pyrolysis of zinc acetylacetonate, zinc silicate is formed (as well as the carbon deposits) upon the reactions between zinc compounds and silica gel surface. CS_{Zr2} and CS_{Ti} include zirconia (~4 nm) and titania (anatase crystallites ~11 nm), respectively. The crystallite sizes were estimated using the Scherrer equation. Note that the sizes of X crystallites are larger than the average pore size of initial Si–60 (Table 2, $\langle R_V \rangle$ and $\langle R_S \rangle$); i.e., a major portion of deposit should be formed on the outer surfaces of silica gel particles or in broad meso/macropores visible in TEM image of initial silica gel (Figs. 2a and 3).

Table 2. Textural characteristics of unmodified and modified silica gel.

Sample	S_{BET} m^2/g	S_{nano} m^2/g	S_{meso} m^2/g	S_{macro} m^2/g	S_{NLDFT} m^2/g	V_p cm^3/g	V_{nano} cm^3/g	V_{meso} cm^3/g	V_{macro}, cm^3/g	$\langle R_V \rangle$ nm	$\langle R_S \rangle$ nm
Si–60	370	130	240	0	362	0.753	0.067	0.686	0	3.52	2.64
CS1	339	151	188	0.1	330	0.718	0.100	0.612	0.006	4.20	2.51
CS2	296	60	222	0	281	0.606	0.016	0.366	0.224	18.22	4.77
CS3	275	51	208	16	260	0.566	0.013	0.281	0.272	22.65	5.33
CS_{Ti}	192	48	142	2	202	0.419	0.012	0.301	0.106	24.10	4.56
CS_{Cr1}	278	125	152	1	256	0.443	0.048	0.344	0.050	8.35	2.45
CS_{Cr2}	293	76	210	7	276	0.622	0.021	0.415	0.190	17.09	4.19
CS_{Co}	187	33	138	16	214	0.524	0.007	0.268	0.248	20.94	6.82
CS_{Ni}	263	57	196	10	258	0.566	0.013	0.347	0.206	19.07	4.82
CS_{Zn}	212	38	167	7	207	0.536	0.009	0.354	0.172	20.72	5.60
CS_{Zr1}	236	82	149	5	213	0.415	0.023	0.288	0.105	13.55	3.64
CS_{Zr2}	281	68	210	3	256	0.537	0.015	0.412	0.110	21.23	4.51

TEM images (Fig. 2) of the initial silica gel and certain carbosils confirm the location of deposits at the outer surface (at least, partially) of silica gel globules. In silica gel globules, there are broad mesopores and macropores (dark areas, Fig. 2a) of 30–85 nm in diameter (Fig. 3), which

could be considered as transport pores appropriate for location of a fraction of the deposits (Fig. 4, Table 2). Note that the MND method with a model of cylindrical pores in silica (described in detail elsewhere [13,60]) is sensitive to broad meso/macropores in pristine silica gel (Fig. 3) in contrast to the DFT methods (Figs. 5a and 6a).

The carbon depositsin CS1 (Fig. 2b) consist of nanoparticles connected with adjacent ones in aggregates. It is fairly homogenous, as only slight differences in darkening of individual areas occupied by carbon deposits are observed. The degree of darkening of these areas depends on the thickness of a carbon layerwith aggregated nanoparticles (the thicker the layer, the darker the area). Some carbon particles can be also formed in broad pores (Figs. 2 and 3) as well as on the outer surfaces of silica gel particles, and as a result, the pore volume and specific surface area of CS decrease in comparison to the silica gel Si–60 (Table 2, *V* and *S*).

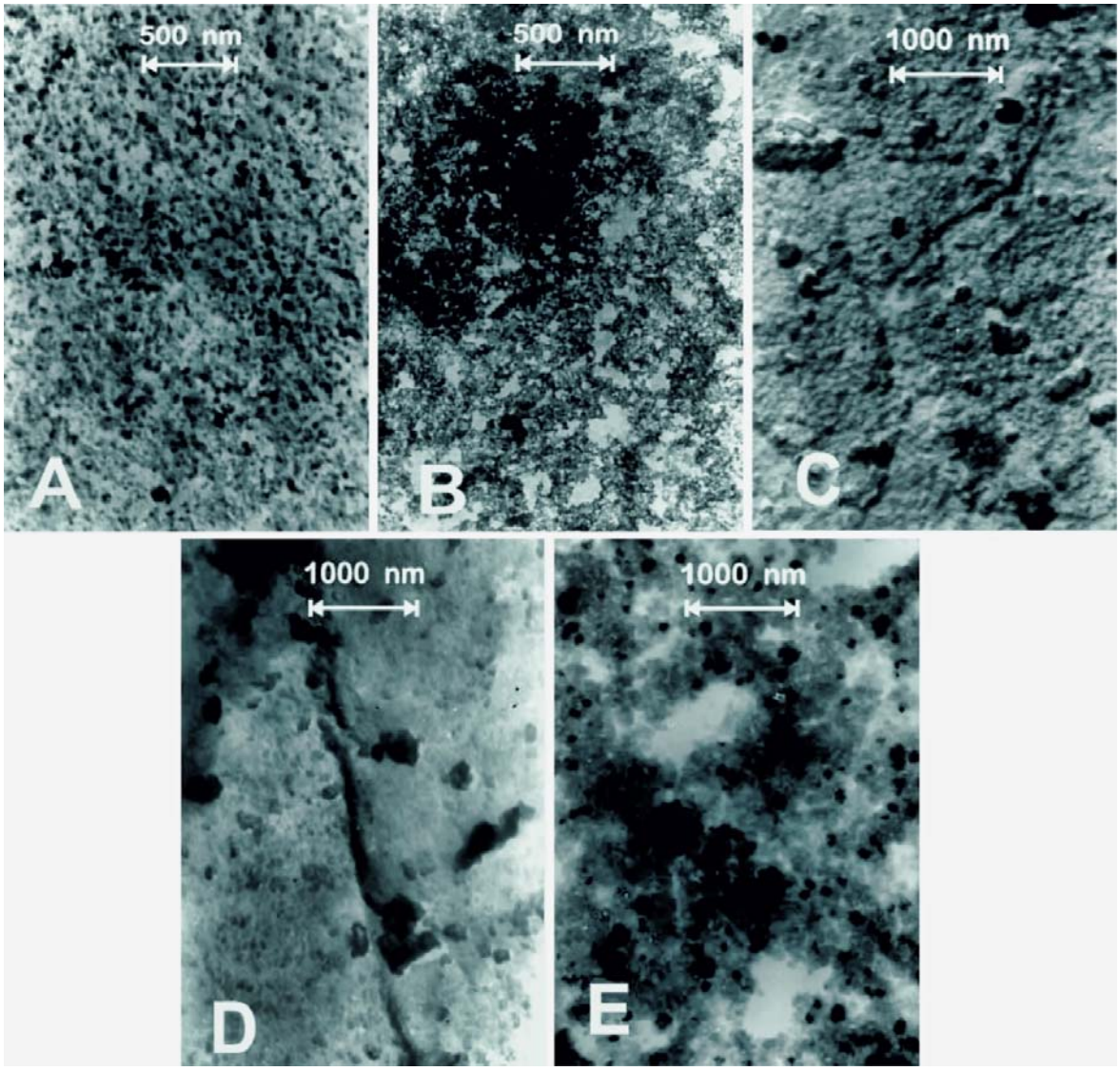

Fig. 2. TEM micrographs of (a) silica, (b) carbosil CS1, (c) CS_{Co}, (d) CS_{Ti}, and (e) CS_{Ni}

Changes in whole adsorbent structure upon the $M(AcAc)_n$ carbonization(giving CS_X) in comparison to that of CS1 are visible in images of CS_{Co} (Fig. 2c), CS_{Ti} (Fig. 2d), and CS_{Ni} (Fig. 2e). The features of X distribution reflect in the C/X morphology (Fig. 2), structure (Table 1), and

texture (Figs. 3–6, Table 2). For example, more nonuniform and denser carbon deposits are observed for CS_{Ti} and the opposite result is for CS_{Zn} (TEM micrograph of CS_{Zn} is not shown here) that can be caused by the difference not only in the catalytic impact of the X phase on the carbonization reactions but also in the features of the phase distributions on the substrate. For example, the $Zn(AcAc)_2$ carbonization leads to the formation of a zinc–silicate phase due to the reactions with a silica surface. The pyrolysis of $TiO(AcAc)_2$ results in the formation of anatase crystallites. Typically, titania deposited on a silica surface represents a segregated phase with relatively weak contacts with a support [13]. Anatase particles (~11 nm) can from on the outer surfaces or in transport pores (Fig. 3) of silica gel particles (0.1–0.2 mm in diameter).

The nitrogen adsorption–desorption isotherms, recorded at 77.35 K (Fig. 1),demonstrate such features as adsorption diminution in a broad range of p/p_0 values that are caused by significant changes in the porosity and specific surface area of modified silica gel samples due to any C/X deposits. These effects depend on both C_C and C_X values, morphology and texture of the deposits and whole adsorbents (Table 2, Figs. 4–6).Thus, the carbonization of acetylacetone or $M(AcAc)_n$ is responsible for various decreases in the adsorbent porosity and accessible surface area in comparison to the characteristics of initial silica gel (Table 2, V, S). The average pore radii(Table 2, $\langle R_V \rangle$) increase for CS samples, but changes in the $\langle R_S \rangle$ values are much smaller because a lion's share of the specific surface area is linked to narrow pores of a much larger number than a number of broad pores significantly contributing the pore volume.

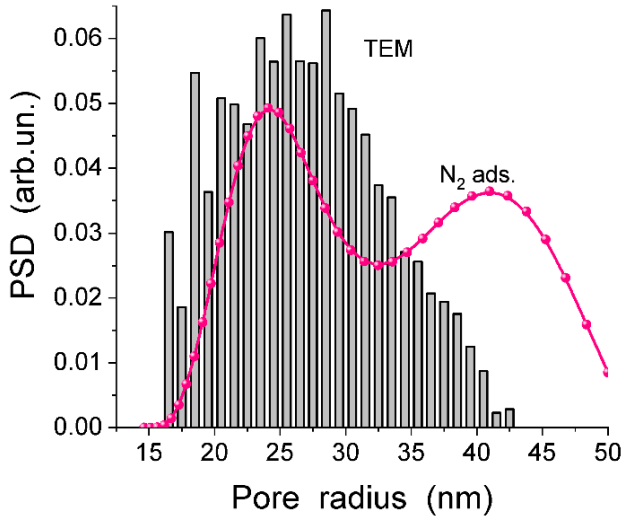

Fig. 3. Pore size distribution for Si–60 calculated using TEM image (Fig. 2a) with ImageJ software (granulometry plugin, ImageJ. Version 1.53u. 2022. (https://imagej.nih.gov/ij/, https://imagej.nih.gov/ij/plugins/granulometry.html); a part of the PSD based on N_2 adsorption is computed using a model cylindrical pores in silica with the MND method [13,60] (giving 0.025, 0.681, and 0.048 cm^3/g for V_{nano}, V_{meso}, and V_{macro}, respectively, and 90, 278, and 2 m^2/g for S_{nano}, S_{meso}, and S_{macro}, respectively)

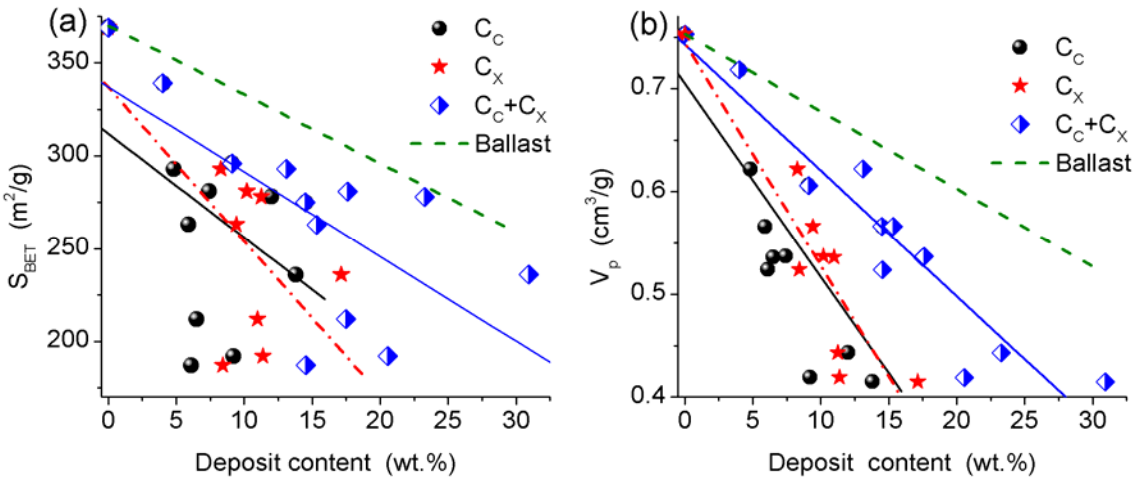

Fig. 4. Decrease in the values of (a) S_{BET} and (b) V_p vs. content of deposits

These morphological and textural effects could be considered as evidence of complicated structure of particles (both of deposits and modified silica globules) and pores in C/X/SiO_2, as tiny C/X particles can be grafted in meso/macropores of silica gel, but larger C/X ones can be formed on the outer surfaces of silica particles with partial blocking of pores (Figs. 2–6) (which can be more effective for narrower pores), and certain changes in the silica pore walls (e.g., due to the Zn silicate formation). Additionally, deposits have own porosity, at least, due to voids between deposit nanoparticles Fig. 2) possessing certain surface area. As a whole, the interior porosity of deposit nanoparticles is low since the total specific surface area of CS_X decreases (Table 2, Figs. 5 and 6). The changes in the morphology and texture of composites increase with increasing deposit content (Fig. 4, Table 2). Note that in the case of the formation of the deposits only in pores, the V and $<R>$ values should decrease simultaneously and the PSD peaks should shift toward lower R values. However, similar simple effects are not observed for any CS sample (Table 2, Figs. 5 and 6).

For CS1, CS2, and CS3, the maximal diminutions are observed for S_{nano} and V_{nano} (Table 2). This effect is clearly visible for IPSD (Fig. 5a,f). There is a certain shift of the main PSD peak of mesopores toward larger pore radius for IPSD with respect to the pore volume (Figs. 5a,f and 6a,f) and specific surface area (Figs. 5f–j and 6f–j). This can be caused by partial decomposition (hydrolysis by water formed upon carbonization of acetylacetone) of the silica pore walls. In the $IPSD_V$ (Fig. 5a), a peak of meso/macropores appears for CS2 and CS3. Similar peaks appear for all CS_X samples (Fig. 5a–e) with one exception for CS1 with a minimal content of carbon deposits (Table 1). Main mesopores in silica gel globules could be linked to broad mesopores and macropores (Fig. 3). Therefore, the pore blocking by the deposits could occur not only at the outer surface of globules but also in the globule interior (around entrances into mesopores located in broad meso/macropores and this process could be more effective for narrower mesopores). Therefore, there are several tendencies in changes in the PSD shape and position of the peak of main mesopores characteristic for the initial silica gel. The maximal shift of the main mesopore peak toward larger pores is observed for CS_{Zn} because of the reactions of $Zn(AcAc)_2$ with the silica pore walls to form zinc silicate that leads to the mesopore broadening. Note that a decrease in the S_{BET} and V_p values vs. C_X is characterized by a larger slope than that forC_C (Fig. 4) because the true density of the X phases is much greater than that of carbon.

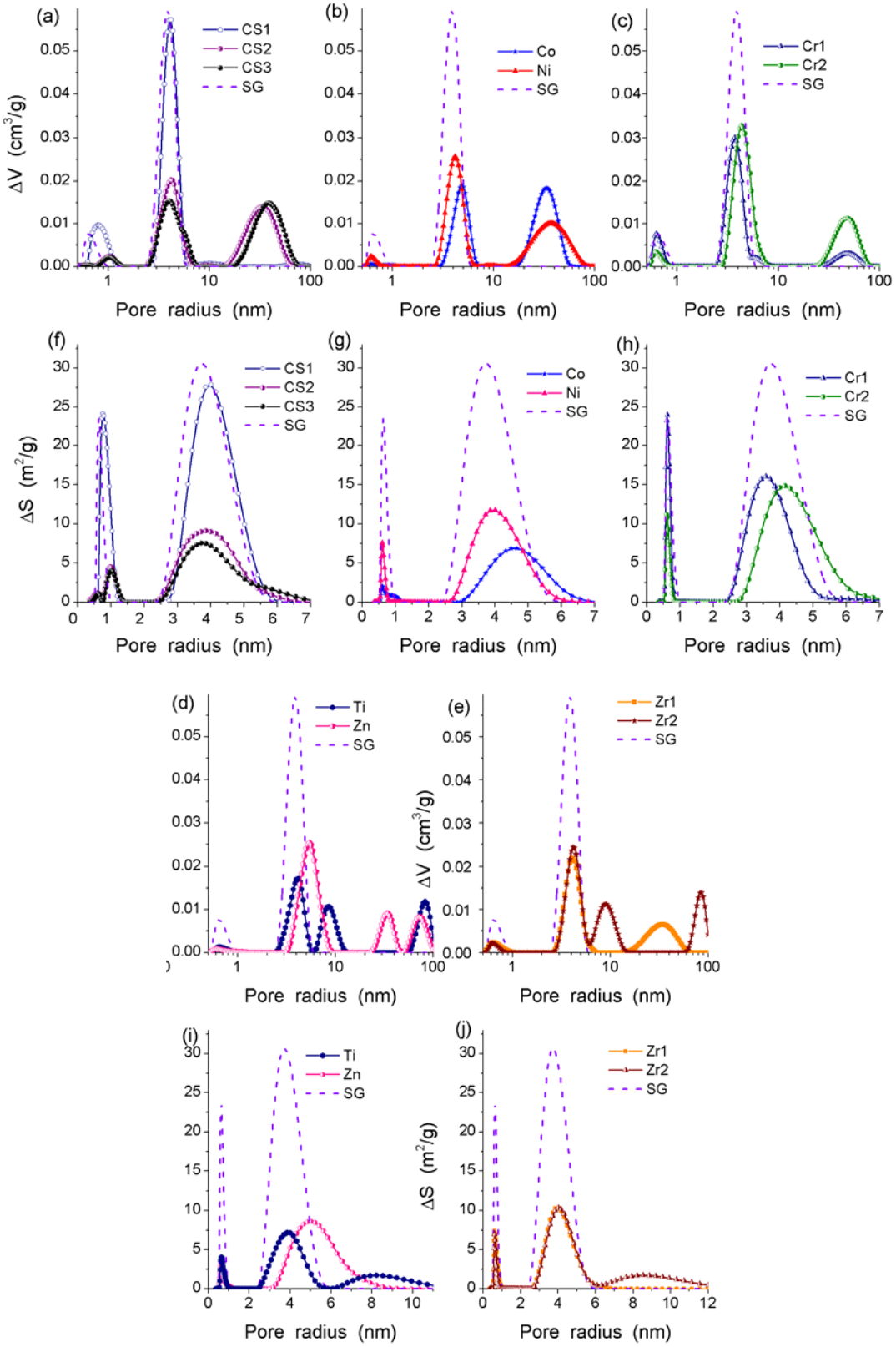

Fig. 5. Incremental pore size distributions calculated using a model of cylindrical pores for SG and DFT VCV/SCR for CS samples with respect to (a–e) the pore volume and (f–j) the specific surface area

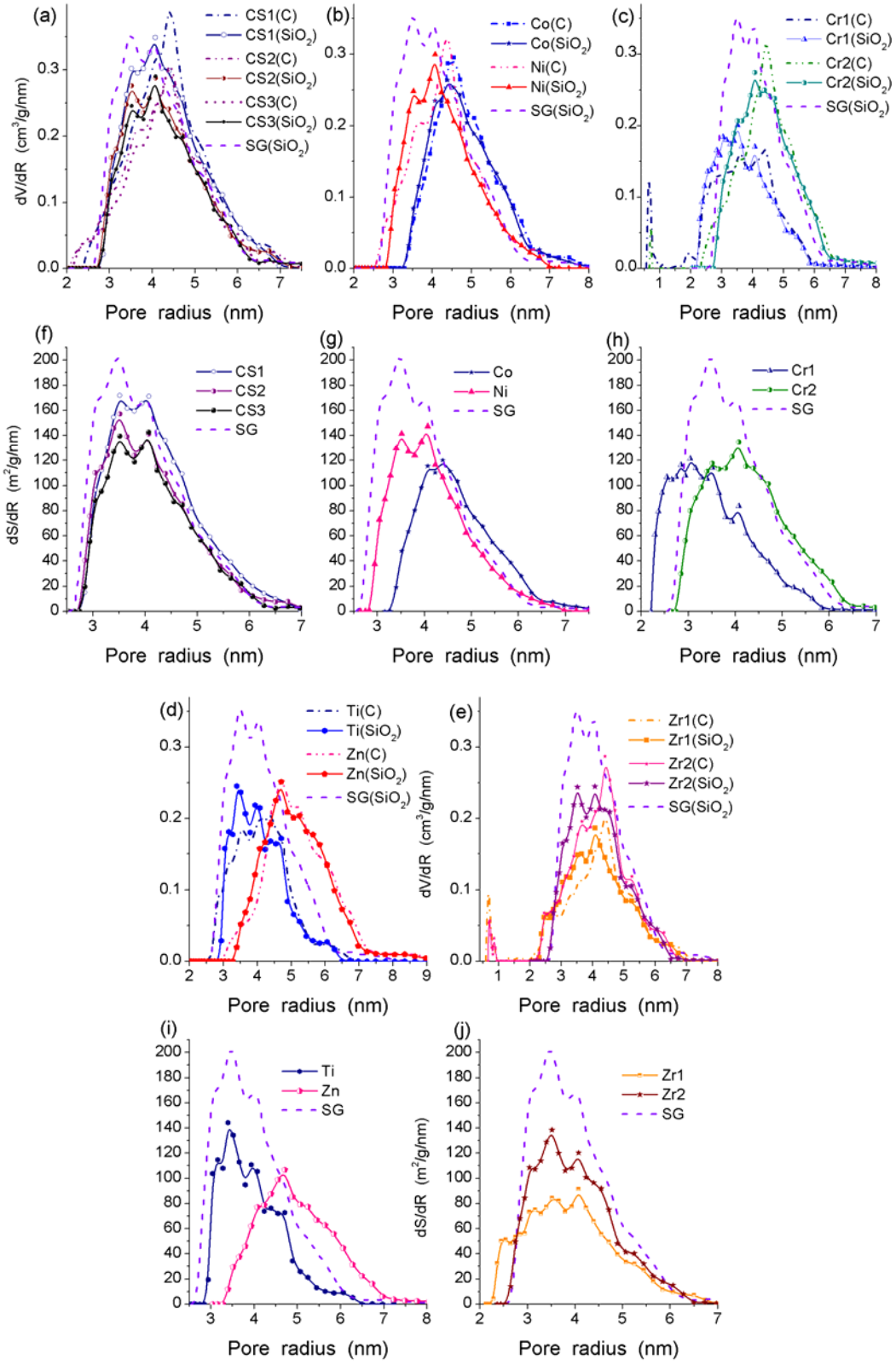

Fig. 6. Differential pore size distributions calculated using the NLDFT method with a model of cylindrical pore in silica (SiO_2) and slit/cylindrical pores in carbon (C) with respect to (a–e) the pore volume and (f–j) the specific surface area

This effect also suggests that the deposits partially play a role of the ballast (pure ballastas a separate nonporous phase does not contribute the porosity and specific surface area but with no blockingof pores). As a whole, the correct textural analysis should be based on the dependence of the characteristics vs. only$C_\Sigma = C_C + C_X$(Fig. 4) since only pure char phase is in CS1, CS2, and CS3 samples; i.e., it is impossible to separate the C_C and C_X values for CS_X samples. Note that the ballast line is located above the composite lines (Fig. 4) and its course has a smaller slope because real deposits block the entrances into a certain part of pores and could be formed in broad pores. Uniform blocking of pores without contribution to the porosity and specific surface area should result in only decreasing PSD intensity without shifting peaks. However, similar results are absent for practically all samples, only CS_{Zr2} demonstrates the PSD changes caused mainly by pore blocking. The PSD for CS_{Cr1} and CS_{Zr1} (Figs. 5 and 6) show that a fraction of the deposits is formed in pores since there is a shift of the PSD toward smaller pore sizes (partially this could be due to contribution of own porosity of deposits). As a whole, there is a complex picture of the changes in the textural characteristics of the composites in a broad range of pore sizes.

Features of the C/X/SiO_2 surface structures and whole texture can reflect in the adsorption–desorption of water (Fig. 7). The increments in C_C for SG → CS1 → CS2 → CS3 are close, but water desorption changes nonlinearly (Fig. 8a) and it is minimal for CS3 (C_C> 10 wt.% is a crucial value for the structure of carbon deposits [13]) when a marked portion of the silica surface is covered by char and a portion of pores can be blocked by carbon particles more hydrophobic than pristine silica surface. The main desorption occurs at 100 °C (Fig. 7) because water is weakly bound in mesopores or unbound in broad mesopores and macropores. Significant changes in the shape of the TG curves (Fig. 7) are observed only for CS_{Cr1} and CS_{Zr1} having maximal concentrations of C/X (Table 1). A decrease in the amounts of adsorbed water correlates with a diminution of the pore volume (Fig. 8d, fitting coefficient $\rho = 0.911$) with growth of deposit filling pores. Correlation between the amounts of desorbed water and the specific surface area is worse (Fig. 8c, $\rho = 0.652$), as the amount of desorbed water is mainly linked to the accessible pore volume.

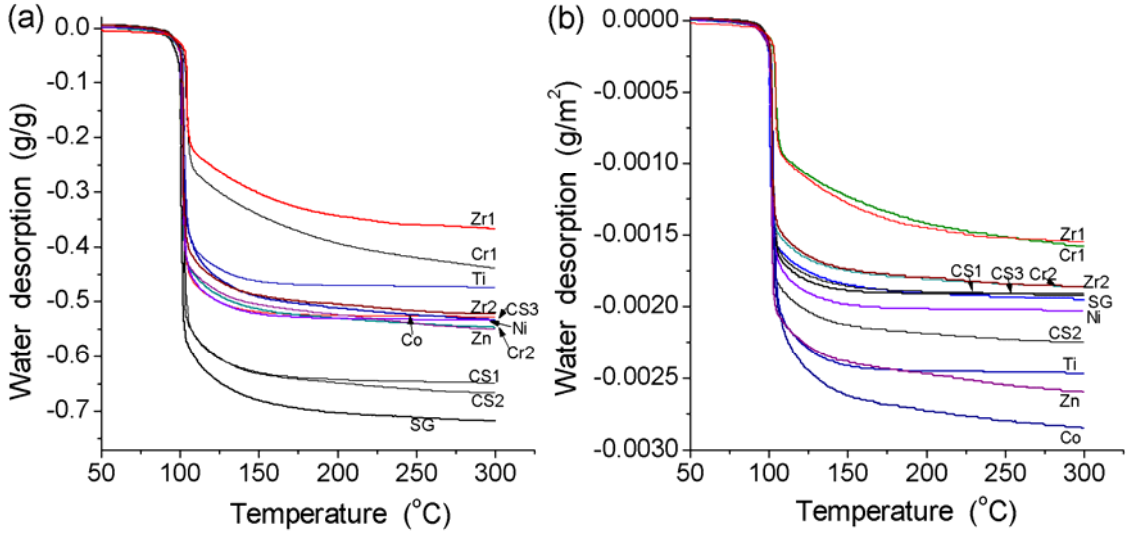

Fig. 7. Desorption of water (TG) as a function of temperature in (a) gram of water per gram of adsorbent and (b) gram of water per m^2 of adsorbent

However, the amounts of water and other compounds desorbed upon heating to 300 °C (Fig. 7a) could be slightly smaller or larger than the pore volume (Table 3). There is no correlation between the values of C_Σ and $\gamma = d/\rho_w/V_p$ that can be caused by several factors: hydrophobicity/hydrophilicity, PSD, pore length and accessibility, chemical reactions upon heating

to 300 °C. Physisorbed water is mainly desorbed at T< 150 °C, and the main weight loss is at 100 °C independent of the adsorbent structure. The desorption upon heating from 150 °C to 300 °C is not great (Table 3, $d_{300} - d_{150}$),and there is no a simple correlation of this value with the deposit contents. Thus, the pore volume plays an important role on the adsorption/desorption of water, but other structural and textural characteristics could affect the desorption processes that results in certain scatter of the amounts of desorbed water vs. any textural characteristic of the adsorbents.

Table 3. Relationship between the pore volume and TG data at 300 °C.

Sample	V_p (cm^3/g)	C_C, wt.%	$C_\Sigma = C_C + C_X$, wt.%	Desorption (d_{300}) at 300°C (g/g)	$\gamma = d_{300}/\rho_w/V_p$	Desorption (d_{150}) at 150°C (g/g)	$d_{300} - d_{150}$ (g/g)
Si–60	0.753	0	0	0.717	0.952	0.680	0.037
CS1	0.718	4.0	4.0	0.649	0.904	0.630	0.019
CS2	0.606	9.1	9.1	0.667	1.101	0.632	0.035
CS3	0.566	14.5	14.5	0.527	0.931	0.519	0.008
CS_{Ti}	0.419	9.2	20.57	0.474	1.131	0.463	0.011
CS_{Cr1}	0.443	12.0	23.26	0.439	0.991	0.342	0.097
CS_{Cr2}	0.622	4.8	13.08	0.546	0.878	0.513	0.033
CS_{Co}	0.524	6.1	14.52	0.533	1.017	0.491	0.042
CS_{Ni}	0.566	5.9	15.32	0.534	0.943	0.522	0.012
CS_{Zn}	0.536	6.5	16.48	0.550	1.026	0.505	0.045
CS_{Zr1}	0.415	13.8	30.94	0.367	0.884	0.302	0.065
CS_{Zr2}	0.537	7.4	17.59	0.522	0.972	0.488	0.034

Note. ρ_w is the density of water.

One could assume that the char content has a stronger effect on the water adsorption than C/X as a whole, as the angle between the line of a linear approximation $C_{water}(C_C)$ and the X axis is greater than that for $C_{water}(C_\Sigma)$ (Fig. 8a). However, this is rather apparent effect for CS_X samples because the X phase affects the $C_{water}(C_C)$ dependence. As a whole, the water adsorption (or desorption observed in the TG measurements, Fig. 7) practically linearly decreases with increasing the C_Σ value causing increasing pore infilling and blocking by deposit particles. Correlation between the deposit amounts and adsorbed/desorbed water amount per m^2 of the surface area of adsorbents is practically absent (Fig. 8b). This is due to the fact that the volume plays the main role in the water adsorption but not the specific surface area since water adsorption occurs through the pore volume infilling mechanism but not by the monolayer adsorption. Notice that obtained results suggest the complicated relationships between the C_C, C_Σ, V, and S values and the amounts of adsorbed water due to nonuniformity of the changes in the C/X/SiO_2surface structures and pore size distributions both important for the water adsorption. The adsorption of water is determined not only by the pore volume or specific surface area but also by the nature of the active surface sites and surface fractality (roughness, small–scale nonuniformity). However, the latter is responsible for minor effects (causing certain scatter in the related dependence, Fig. 8) but the pore volume is the main factor determining the course of the water adsorption/desorption (Fig. 8d).

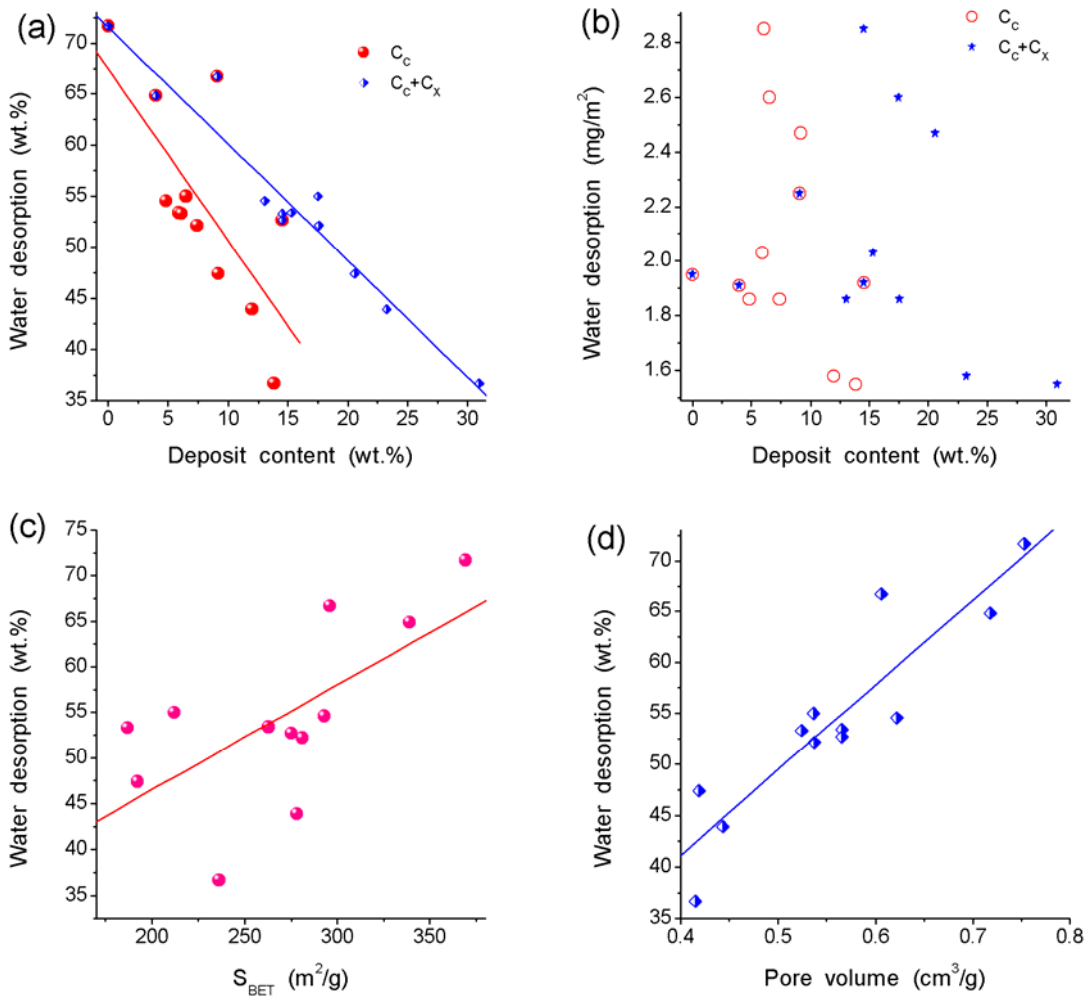

Fig. 8. Relationships between the amounts of desorbed water (in wt. % and mg/m^2) (a, b) C_C and $C_\Sigma = C_C + C_X$ values, (c) specific surface area, and (d) pore volume.

Conclusion

On the basis of obtained results, one can conclude that C/X depositson silica gel Si–60 affect nonlinear dependencies of the morphological and textural characteristics of whole hybrid C/X/silica adsorbents on the C_Σ values. The simultaneous appearance of the C and X phases is responsible for more complicated relationships between the adsorbent characteristics and deposit amounts. It can enhance a small–scale nonuniformity of the whole surface that reflects in changes in the pore size distribution and adsorption/desorption of water. These effects are caused by variations in the nature (carbon, metal oxide, silicate, and metal possessing different catalytic capabilities in pyrolysis) and structure (sizes of crystallites, amorphous oxide or silicate particles as well as carbon ones and their distribution on silica gel substrate, in pores or on outer surface) of C and X phases in C/X/silica gel adsorbents. There is a tendency of a reduction in the adsorbent porosity and specific surface area with growing amounts of the C/X deposits. A correlation between the content of the grafted phases and pore volume is closer to a linear one than that for the specific surface area. The appearance of C or C/X deposits typically leads to broadening of the pore size distributions. However, for some C/X/SiO_2 adsorbents, then an oporosity decreases more strongly with increasing deposit content. The largest pores are observed in the PSD for the composites

computed using the nitrogen adsorption with the DFT VCV/SCR method in contrast to those computed with the NLDFT method. Grafting of C/X leads to the transformations not only of broad meso/macropores(observed at the outer surface of initial silica globules) but also of mesopores in the globule in terior. The deposits at the outer surface of Si-60 cause significant changes in the average values of the pore radii $<R_V>$. The amounts of water adsorbed onto $C/X/SiO_2$ decrease with increasing deposit content, and the content ofthe carbon phase (mainly hydrophobic)could play an important role in reduction of the water adsorption than the X phase (mainly hydrophilic) does. Therefore, there is no simple relationships between efficiency of pore infilling by water and the total amounts of the deposits. In future, it is of interest to prepare hybrid adsorbents using a mixture of different organometallics and substrates of different origin.

References

[1] Yang R.T. *Adsorbents: Fundamentals and Applications*. (New York: Wiley, 2003).

[2] Birdi K.S. (Ed.) *Handbook of Surface and Colloid Chemistry*. Third edition. (Boca Raton: CRC Press, 2009).

[3] *Ullmann's Encyclopedia of Industrial Chemistry*. (Weinheim: Wiley–VCH, 2008).

[4] Somasundaran P. (Ed.) *Encyclopedia of Surface and Colloid Science*. Third Edition. (Boca Raton: CRC Press, 2015).

[5] Ahuja S. (Ed.) *Separation Science and Technology.* Vol. 15. (Amsterdam: Elsevier, 2022).

[6] Hussain C.M. (Ed.) *Handbook of Polymer Nanocomposites for Industrial Applications*. (Amsterdam: Elsevier, 2021).

[7] Ahmad A., Kumar R., Jawaid M. (Eds.) *Emerging Techniques for Treatment of Toxic Metals from Wastewater*. (Amsterdam: Elsevier, 2022).

[8] S. Singh, P. Kumar, D.P. Mondal (Eds.) *Advanced Ceramics for Versatile Interdisciplinary Applications*. (Amsterdam: Elsevier, 2022).

[9] Ngu L.H. *Carbon Capture Technologies*. (Amsterdam: Elsevier, 2022).

[10] Lu K. *Nanoparticulate Materials. Synthesis, Characterization, and Processing.* (Hoboken, New Jersey: John Wiley & Sons, Inc., 2013).

[11] Moreno–Piraján J.C., Giraldo–Gutierrez L., Gómez–Granados F. *Porous Materials Theory and Its Application for Environmental Remediation*. (Cham: Springer Nature, 2021).

[12] Rousseau R.W. *Handbook of Separation Process Technology*. (New York: John Wiley & Sons, 1987).

[13] Gun'ko V.M., Turov V.V. *Nuclear Magnetic Resonance Studies of Interfacial Phenomena*. (Boca Raton: CRC Press, 2013).

[14] Leboda R. Carbon–mineral adsorbents – new type of sorbents. Part I. The methods of preparation. *Mater. Chem. Phys.* 1992. **31**: 243. Part II. Surface properties and methods of their modification *Mater. Chem. Phys*. 1993. **34**: 123.

[15] Chan Z., Miao F., Xiao Z., Juan H., Hongbing Z. Effect of doping levels on the pore structure of carbon nanotube/silica xerogel composites. *Mater. Lett.*2007. **61**: 644.

[16] Lavorgna M., Romeo V., Martone A., Zarrelli M., Giordano M., Buonocore G.G., Qu M.Z., Fei G.X., Xia H.S. Silanization and silica enrichment of multiwalled carbon nanotubes: Synergistic effects on the thermal–mechanical properties of epoxy nanocomposites. *European Polymer J.*2013. **49:** 428.

[17] Othman R.N., Kinloch I.A., Wilkinson A.N. Synthesis and characterisation of silica–carbon nanotube hybrid microparticles and their effect on the electrical properties of poly(vinyl alcohol) composites. *Carbon.*2013. **60**: 461.

[18] Choi S., Kim K., Nam J., Shim S.E. Synthesis of silica–coated graphite by enolization of poly vinyl pyrrolidone and its thermal and electrical conductivity in polymer composites. *Carbon.*2013. **60**: 254.

[19] Chu Y.–H., Yamagishi M., Wang Z.–M., Kanoh H., Hirotsu T. Adsorption characteristics of nanoporous carbon–silica composites synthesized from graphite oxide by a mechanochemical intercalation method. *J. Colloid Interface Sci*.2007. **312**: 186.
[20] Wang Z.–M., Shishibori K., Hoshinoo K., Kanoh H., Hirotsu T. Examination of synthesis conditions for graphite–derived nanoporous carbon–silica composites. *Carbon.*2006. **44**: 2479.
[21] Kumagai S., Ishizawa H., Aoki Y., Toida Y. Molded micro– and mesoporous carbon/silica composite from rice husk and beet sugar. *Chem. Eng. J.* 2010. **156**: 270.
[22] Tso C.Y., Chao C.Y.H. Activated carbon, silica–gel and calcium chloride composite adsorbents for energy efficient solar adsorption cooling and dehumidification systems. *Int. J. Refrigeration.* 2012. **35**: 1626.
[23] Ye L., Ji Z.–H., Han W.–J., Hu J.–D., Zhao T. Synthesis and characterization of silica/carbon composite aerogels. *J. Am. Ceramic Soc*. 2010. **93**: 1156.
[24] Furtado A.M.B., Wang Y., LeVan M.D. Carbon silica composites for sulfur dioxide and ammonia adsorption. *Micropor. Mesopor. Mater.* 2013. **165**: 48.
[25] Glover T.G., LeVan M.D. Carbon–silica composite adsorbent: Sensitivity to synthesis conditions. *Micropor. Mesopor. Mater*. 2009. **118**: 21.
[26] Valle–Vigón P., Sevilla M., Fuertes A.B. Carboxyl–functionalized mesoporous silica–carbon composites as highly efficient adsorbents in liquid phase. *Micropor. Mesopor. Mater*. 2013. **176**: 78.
[27] Santa C.F., Jaber M., Guth J.L., Sierra L. Synthesis of texturally biphasic mesoporous carbon–silica composites and carbons. *Micropor. Mesopor. Mater*. 2013. **173**: 53.
[28] Lua A.C., Shen Y. Preparation and characterization of polyimide–silica composite membranes and their derived carbon–silica composite membranes for gas separation. *Chem. Eng. J.* 2013. **220**: 441.
[29] Sanchez F., Ince C. Microstructure and macroscopic properties of hybrid carbon nanofiber/silica fume cement composites. *Compos. Sci. Technol*. 2009. **69**: 1310.
[30] Zhou X., Shi T. One–pot hydrothermal synthesis of a mesoporous SiO_2–graphene hybrid with tunable surface area and pore size. *Appl. Surf. Sci*. 2012. **259**: 566.
[31] Nandan D., Sreenivasulu P., Sivakumar Konathala L.N., Kumar M., Viswanadham N. Acid functionalized carbon–silica composite and its application for solketal production. *Micropor. Mesopor. Mater*. 2013. **179**: 182.
[32] Xu H., Zhang H., Huang Y., Wang Y. Porous carbon/silica composite monoliths derived from resorcinol–formaldehyde/TEOS. *J. Non–Crystal. Solid*. 2010. **356**: 971.
[33] Charmas B. Characterization of porosity and thermal properties of Ni–doped carbosils obtained by starch gelation. *Adsorption Science & Technology*. 2015. **33**: 539.
[34] Meti P., Mahadik D.B., Lee K.–Y., Wang Q., Kanamori K., Gong Y.–D., Park H.–H. Overview of organic–inorganic hybrid silica aerogels: Progress and perspectives. *Materials & Design.* 2022. **222**: 111091.
[35] Ounphikul B., Chantarasombat N., Hunt A.J., Ngernyen Y. A new low–cost carbon–silica composite adsorbent from a by–product of the sugar industry. *Materials Today: Proc*. 2022. **51**: 1884.
[36] Gun'ko V.M., Matkovsky A.K., Charmas B., Skubiszewska–Zięba J., Pasieczna–Patkowska S., Carbon–silica gel adsorbents: effects of matrix structure and carbon content on adsorption of polar and nonpolar adsorbates. *J. Thermal Analysis and Calorimetry*. 2017, **128**: 1683.
[37] Leboda R., Turov V.V., Charmas B., Skubiszewska–Zięba J., Gun'ko V.M. Surface properties of mesoporous carbon–silica gel adsorbents. *J. Colloid Interface Sci*. 2000. **223**: 112.

[38] Gun'ko V.M., Leboda R., Skubiszewska–Zięba J., Rynkowski J. Silica gel modified due to pyrolysis of acetylacetone or metal (Ti, Cr, Co, Ni, Zn, Zr) acetylacetonates. *J. Colloid Interface Sci.* 2000. **231**: 13.
[39] Gun'ko V.M., Leboda R., Turov V.V., Villiéras F., Skubiszewska–Zięba J., Chodorowski S., Marciniak M. Structural and energetic nonuniformities of pyrocarbon–mineral adsorbents. *J. Colloid Interface Sci*. 2001. **238**: 340.
[40] Gun'ko V.M., Leboda R., Skubiszewska–Zięba J., Turov V.V., Kowalczyk P. Structure of silica gel Si–60 and pyrocarbon/silica gel adsorbents thermally and hydrothermally treated. *Langmuir*. 2001. **17**: 3148.
[41] Gun'ko V.M., Leboda R., Pokrovskiy V.A., Charmas B., Turov V.V., Ryczkowski J. A study of the organic carbon content of silica gel carbonised by pyrolysis of alcohols. *J. AnalyticalAppliedPyrolysis*. 2001. **60**: 233.
[42] Skubiszewska–Zięba J., Leboda R., Seledets O., Gun'ko V.M. Effect of preparation conditions of carbon–silica adsorbents based on mesoporous silica gel Si–100 and carbonised glucose on their pore structure. *Colloids Surf. A: Physicochem. Eng. Aspects*. 2003. **231**: 39.
[43] Gun'ko V.M., Skubiszewska–Zięba J., Leboda R., Turov V.V. Impact of thermal and hydrothermal treatments on structural characteristics of silica Gel Si–40 and carbon/silica gel adsorbents. *Colloids Surf. A: Physicochem. Eng. Aspects*. 2004. **235**: 101.
[44] Seledets O., Gun'ko V.M., Skubiszewska–Zięba J., Leboda R., Musiatowicz M., Podkoscielny P., Dabrowski A. Structural and energetic heterogeneities of pyrocarbon/silica gel systems and their adsorption properties. *Appl. Surf. Sci.* 2005. **240**: 222.
[45] Gun'ko V.M., Seledets O., Skubiszewska–Zięba J., Zarko V.I., Leboda R., Janusz W., Chibowski S. Phosphorus–containing carbon deposits on silica gel Si–100. *Micropor. Mesopor. Mater.* 2005.**87**: 133.
[46] BlitzJ.P., Gun'koV.M. (Eds.)*Surface Chemistry in Biomedical and Environmental Science.*NATO Science Series II: Mathematics, Physics and Chemistry. Vol. 228 (Dordrecht: Springer,2006).
[47] Skubiszewska–Zięba J., Charmas B., Leboda R., Gun'ko V.M. Carbon–mineral adsorbents with a diatomaceous earth/perlite matrix modified by carbon deposits. *Micropor. Mesopor. Mater.* 2012. **156**: 209.
[48] Tomaszewski W., Gun'ko V.M.,Skubiszewska–Zięba J., Charmas B., Leboda R. Influence of carbon deposits and subsequent silylation of silica gel on sorption efficiency of explosive nitramines. *ColloidsSurf. A: Physicochem. Eng. Aspects*. 2015. **468**: 76.
[49] Tomaszewski W., Gun'ko V.M. Evaluation of adsorption and desorption steps in solid–phase extraction of explosives using carbon/silica gel nanocomposites. *J. Separ. Sci*. 2015. **38**: 2488.
[50] Leboda R., Marciniak M., Gun'ko V.M., Grzegorczyk W., Malygin A.A.,Malkov A.A. Structure of carbonized mesoporous silica gel/ CVD–titania.*Colloids Surf. A: Physicochem. Eng. Aspects*. 2000.**167**: 275.
[51] Gun'ko V.M., Leboda R., Marciniak M., Grzegorczyk W., Skubiszewska–Zięba J.,Malygin A.A.,Malkov A.A. CVD–titania/silica gel carbonized due to pyrolysis of cyclohexene.*Langmuir.* 2000.**16**: 3227.
[52] Gun'ko V.M., Leboda R., Charmas B., Villieras F. Characterization of spatial and energetic structures of carbon–silica gels.*Colloids Surf. A: Physicochem. Eng. Aspects*. 2000.**173**: 159.
[53] Gun'ko V.M., Villiéras F., Leboda R., Marciniak M., Charmas B., Skubiszewska–Zięba J., Characterization of CVD–titania/silica gel by means of low pressure nitrogen adsorption.*J. Colloid Interface Sci.* 2000.**230**: 320.

[54] Leboda R., Gun'ko V.M., Skubiszewska–Zięba J., Gierak A., Oleszczuk P. Properties of thin polythylene glycol layers on the surface of silica gel and pyrocarbon/silica gel. Effect of topography and morphology of carbon deposit.*Mater. Chem. Phys*. 2001.**70**: 25.
[55] Gun'ko V.M., Leboda R., Turov V.V., Charmas B., Skubiszewska–Zięba J. Structural and energetic heterogeneities of hybrid carbon–mineral adsorbents. *Appl. Surf. Sci*. 2002. **191**: 286.
[56] Gun'ko V.M., Turov V.V., Skubiszewska–Zięba J., Charmas B., Leboda R. Structural and adsorptive characteristics of pyrocabon/silica gel Si–60.*Adsorption*. 2004.**10**: 5.
[57] Gun'ko V.M. Confined space effects on various liquids interacting with fumed nanooxides and porous silicas.*Chem. Phys. Technol. Surf*. 2022. **13**: 47.
[58] Gregg S.J., Sing K.S.W. *Adsorption, Surface Area and Porosity*. 2nd ed. (London: Academic Press, 1982).
[59] Adamson A.W., Gast A.P. *Physical Chemistry of Surface*. 6th edition. (New York: Wiley, 1997).
[60] Gun'ko V.M. Textural characteristics of composite adsorbents analyzed with density functional theory and self–consistent regularization procedure. *Chemistry, Physics and Technology of Surface*. 2020. **11**: 163.
[61] Gun'ko V.M. Various methods to describe the morphological and textural characteristics of various materials. *Chemistry, Physics and Technology of Surface.* 2018. **9**: 317.
[62] Gun'ko V.M. Morphological and textural features of various materials composed of porous or nonporous nanoparticles differently packed in secondary structures. *Appl. Surf. Sci.* 2021. **569**: 151117.
[63] Ravikovitch P.I., Neimark A.V. Density functional theory model of adsorption on amorphous and microporous silica materials. *Langmuir.* 2006. **22**: 11171.

ГІБРИДНІ КОМПОЗИТИ СИНТЕЗОВАНІ ПРИ КАРБОНІЗАЦІЇ АЦЕТИЛАЦЕТОНУ ТА АЦЕТИЛАЦЕТОНАТІВ МЕТАЛІВ НА ПОВЕРХНІ СИЛІКАГЕЛЮ

В.М. Гунько[1], Я. Скубішевська-Земба[2], Б. Хармас[2]

[1]Інститут хімії поверхні ім. О.О. Чуйка Національної академії наук України вул. Генерала Наумова, 17, Київ, 03164, Україна, e-mail:vlad_gunko@ukr.net
[2]Хімічний факультет, Університет ім. Марії Кюрі-Склодовської, пл. Марії Кюрі-Склодовської, 3, 20-031Люблін, Польща

Гібридні адсорбенти з вуглецем/кремнеземом, вуглецем/оксидом металу/кремнеземом і вуглецем/металом/кремнеземом можуть бути цікаві з практичної точки зору, оскільки вони можуть ефективно адсорбувати як полярні, так і неполярні сполуки. Тому мезопористий силікагель Si–60, модифікований карбонізацією ацетилацетону або ацетилацетонатів цирконію, титану, нікелю, цинку, хрому та кобальту досліджували за допомогою адсорбції-десорбції азоту та води, термогравіметрії, трансмісійної електронної мікроскопії, рентгенівської дифракції та рентгенівської флуоресценції. Прищеплені фази C/X складаються із сполук металу (X позначає оксид або силікат металу або метал) і вугілля, характеристики яких можна змінювати, змінюючи метал у прекурсорах та їхню кількість при карбонізації. Морфологічні, структурні та текстурні характеристики C/X/SiO_2, такі як склад і розподіл частинок за розміром депозитів, число та сорт полярних та неполярних поверхневих центрів, питома поверхня, об'єм пор та розподіл пор за розмірами залежать від типу і вмісту депозитів C/X. Зміни в прищеплених речовинах відбуваються зі збільшенням концентрації прекурсору та C/X та можливого каталітичного ефекту X-фаз на карбонізацію. Правильний підбір структури та кількості прекурсорів дозволяє контролювати характеристики гібридних адсорбентів, що важливо з практичної точки зору.

Ключові слова:*мезопористийсилікагель, карбонізація ацетилацетонатів металів, вуглецеві депозити, депозити вуглець/сполука металу, морфологія депозитів, текстурні характеристики, десорбція води*